International Journal of Crashworthiness
Publication details, including instructions for authors and subscription information:
http://www.tandfonline.com/loi/tcrs20

The optimisation of the energy absorption of partially Al foam-filled commercial 1050H14 and 6061T4 Al crash boxes

A. K. Toksoy [a] & M. Güden [a]
[a] Dynamic Testing and Modeling Laboratory and Department of Mechanical Engineering, Izmir Institute of Technology, Gulbahce Koyu, Urla, Izmir, Turkey

Available online: 24 Mar 2011

To cite this article: A. K. Toksoy & M. Güden (2011): The optimisation of the energy absorption of partially Al foam-filled commercial 1050H14 and 6061T4 Al crash boxes, International Journal of Crashworthiness, 16:1, 97-109

To link to this article: http://dx.doi.org/10.1080/13588265.2010.514774

International Journal of Crashworthiness
Vol. 16, No. 1, February 2011, 97–109

The optimisation of the energy absorption of partially Al foam-filled commercial 1050H14 and 6061T4 Al crash boxes

A.K. Toksoy and M. Güden*

Dynamic Testing and Modeling Laboratory and Department of Mechanical Engineering, Izmir Institute of Technology, Gulbahce Koyu, Urla, Izmir, Turkey

(*Received 28 May 2010; final version received 9 August 2010*)

Partially Alulight and Hydro Al closed-cell foam-filled commercial 1050H14 Al and 6061T4 Al crash boxes were optimised using the response surface methodology in order to maximise specific energy absorption (SEA). The quasi-static crushing of empty and filled crash boxes was simulated using LS-DYNA, and the results were further confirmed with experimental quasi-static crushing testing of empty and Alulight foam-filled commercial 1050H14 Al crash boxes. Results showed that partial foam filling of commercial crash boxes increased both SEA and mean load because of foam filler axial and lateral deformation in between the progressing folds of the crash box. Within the studied constraint range of box mean load, box wall thickness and foam filler density, the optimised Alulight and Hydro foam-filled 1050H14 and 6061T4 crash boxes resulted in 26%–40% increase in total energy absorption as compared with empty crash boxes. Considering the same weight basis, the use of a higher yield strength box wall material and higher plateau stresses of Al foam filler resulted in higher energy absorptions in partial foam-filled boxes at relatively low displacements.

Keywords: crash box; simulation; Al foam; optimisation; energy absorption

1. Introduction

Al foams are often considered as the lightweight materials for the filling of columns. The foam filling, however, does not always bring about energetically favourable structural elements when compared with empty counterparts. Therefore, an optimisation schedule is often needed in order to reveal the advantages of foam filling. The optimisation of the specific energy absorption (SEA) of the multi-corner thin-walled columns was previously investigated using the response surface methodology (RSM) with several different objective functions including linear, quadratic, cubic and quintic polynomials [9,11]. A minimum error was found, when a quadratic polynomial objective function was used. The examples of the optimisation studies on the crushing of circular and rectangular tubes include the following references [2,4,18]. The shape optimisation of a non-uniform closed-hat front crash absorber section of an automobile was investigated using RSM with rectangular hole-type and circular dent-type crash initiator to maximise the crash energy absorption [5]. A cross-section shape optimisation study was performed using the average mean crushing load as an objective function [7]. The constraint imposed was a constant prismatic cross section, and the optimisation resulted in 91% increase in the energy absorption at an impact velocity of 48 km h^{-1}. The minimum weight optimisation of an Al foam-filled S-frame was carried out using an analytic energy equation as an objective function, and the optimised variables including the thickness and cross-section length of the frame and the foam relative density were further validated by the finite element simulations [10]. An optimisation study was conducted on Alporas Al foam-filled Al tubes to maximise SEA for the crash box applications by taking the cross-section width and foam density as independent variables and a maximum mean crushing load constraint of 68.5 kN [19]. Equivalent SEA values of the optimised empty square tubes were compared with those of the foam-filled Al tube, and an approximately 20% increase in SEA values was found in filled tubes following the optimisation schedule. A similar optimisation study conducted on Al honeycomb-filled Al square tubes resulted in 14.3% increase in SEA values of the filled tube as compared with its empty counterpart [20]. In an optimisation study on the honeycomb-filled bitubular hexagonal columns using Chebyshev's orthogonal polynomial as an objective function and the independent variables of inner side length and the thickness of inner and outer walls yielded 40% increase in SEA values of bitubal honeycomb-filled Al tubes [21]. The bending properties of Alporas Al foam-filled square tubular structures were further optimised [17]. Agreements between experimental and numerical results were found under the defined constraints, and 28.1% increase in SEA values was reported in foam-filled tubular structures.

*Corresponding author. Email: mustafaguden@iyte.edu.tr

ISSN: 1358-8265 print / ISSN: 1754-2111 online

DOI: 10.1080/13588265.2010.514774
http://www.informaworld.com

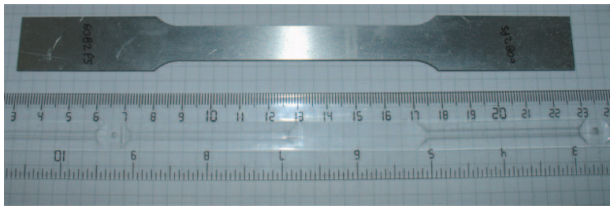

Figure 1. 1050H14 Al tensile test specimen.

Despite few studies on the optimisation of empty and foam-filled tubes, there has been no study in the literature on the optimisation of partially Al foam-filled tubes. The focus in this is therefore on the optimisation of Al closed-cell foam-filled commercial 1050H14 Al crash boxes under a constraint mean crushing load and commercially available tube wall thickness and foam relative density to maximise SEA values. The effects of crash box alloy and foam filler type on SEA values were also investigated for comparison. This study would therefore provide design criteria for the foam filling of commercial automobile crash boxes.

2. Materials and testing

As-received commercial 2-, 2.5- and 3-mm-thick 1050H14 Al crash boxes (73 × 70 × 120 mm) were manufactured by a series of processing routes including laser cutting, bending and TIG welding of 1050H14 Al sheets. The tension test samples (Figure 1) were cut from a 3-mm-thick extruded 1050H14 Al sheet according to ASTM E8/E8M-08 standard [1] using an electro-discharge machine and tested at a quasi-static strain rate of 1.66×10^{-3} s^{-1}. A video extensometer was used to measure the specimen displacement during the tests. Alulight (AlSi10) aluminium closed-cell foam cubic compression test samples of 30 × 30 × 30 mm (Figure 2(a)) were cut from as-received foam panels (625 × 625 × 30 mm). Before compression testing, the weight of each test sample was measured. The tested foam samples densities and relative densities varied between 297 kg m^{-3} and 580 kg m^{-3} and 0.11 and 0.215, respectively. Compression tests were performed at a strain rate of 2.77×10^{-3} s^{-1}, through the thickness direction of as-received foam panels, parallel to the foaming direction as shown in Figure 2(b). The foam compressive stress–strain behaviour was fitted with Deshpande and Fleck foam model [6,14], which is represented by the following relations:

$$\sigma = \sigma_p + \gamma \frac{\varepsilon}{\varepsilon_D} + \alpha_2 \ln\left(\frac{1}{1-(\varepsilon/\varepsilon_D)^{\beta}}\right) \tag{1}$$

and

$$\varepsilon_D = -\frac{9+\alpha^2}{3\alpha^2} \ln(\rho_f/\rho_{fo}), \tag{2}$$

where σ is the stress, ε is the strain, σ_p is the plateau stress, ε_D is the densification strain, γ, α_2, β and α are the constants, ρ_f is the foam density and ρ_{fo} is the density of the foam material. By taking a zero Poisson's ratio for the foam [3], the value of α is calculated as $\sqrt{9/2} = 2.12$. The foam material properties of σ_p, α_2, γ and β are expressed as functions of the foam and foam material density as [8],

$$\left\{\sigma_p, \alpha_2, \gamma, \frac{1}{\beta}\right\} = C_0 + C_1\left(\frac{\rho_f}{\rho_{fo}}\right)^{n'}, \tag{3}$$

where C_0, C_1 and n' are the constants. The constructed Deshpande and Fleck foam model parameters were used to create compressive stress–strain curves of the foam filler in the numerical modelling of filled tubes.

Four V-shaped grooves were formed on the opposite surfaces of the crash boxes, two near the top and two near the bottom of the boxes (Figures 3(a) and 3(b)). The distance between each V-groove on the same face of the boxes was 60 mm. Two layers of foam filler (each 30 mm in thickness) were inserted in between the grooves. As the foam layers were tightly held between the grooves, no bonding agent use was required between the layers of foam fillers and also between foam filler and box wall. The grooves also functioned to fix the foam filler at the middle of the crash

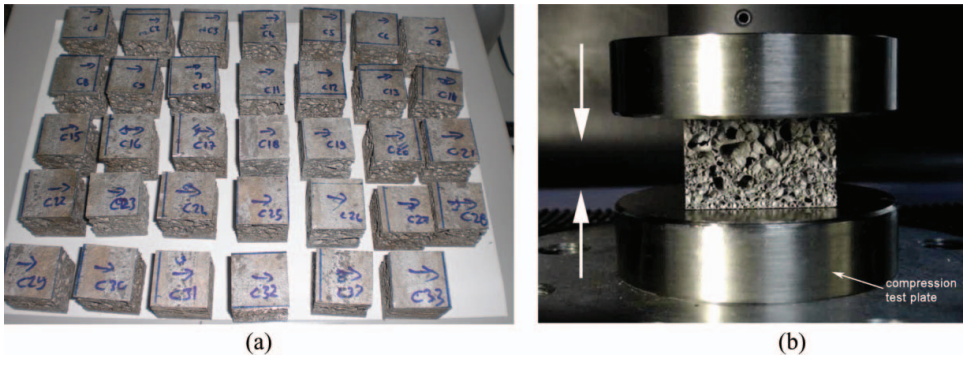

Figure 2. (a) Alulight foam compression test samples and (b) foam compression through thickness direction.

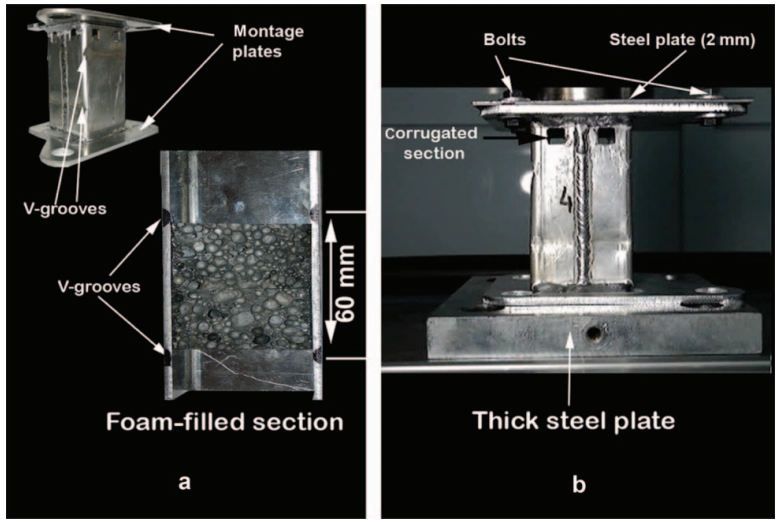

Figure 3. (a) The cross section of a partially foam-filled 3-mm-thick box showing V-grooves on the surface and (b) the picture of a foam-filled crash box in compression testing.

box during compression testing. At the top of the boxes, a corrugated section (two square holes on each face) was intentionally machined in order to form an easy fold initiation site. The compression tests were performed by means of the montage plates welded at the ends of the box (Figure 3(b)). The montage plates were made from the same alloy sheet of the crash boxes, 1050H14 Al, with a thickness of 5 mm.

3. Optimisation methodology

The length and the width of the crash box column were taken constant, while the thickness of the box (t) and the relative density of the foam filler ($\rho^* = \rho_f/\rho_{fo}$) varied in the optimisation study. In addition, the mean load (P_m) value, which determines the level of deformation energy transferred to the passenger compartment, was kept below a prescribed value (P_{critical}). Hence, the optimisation of partial aluminium foam-filled crash box is formulated as,

$$\begin{aligned} &\text{Maximise} : \text{SEA}(t, \rho^*), \\ &\text{Constraints} : P_{\text{m}}(t, \rho^*) \le P_{\text{critical}}, \\ &t_{\text{l}} \le t \le t_{\text{u}}, \quad \rho l\ \rho_{\text{l}}^* \le \rho^* \le \rho_{\text{u}}^*, \end{aligned}$$

where t_l, t_u, ρ_l^* and ρ_u^* are the lower and upper bound values of t and ρ, respectively. The SEA was calculated using the following relation

$$SEA = \frac{\int P\, d\delta}{m_t}, \tag{4}$$

where P is the load, δ is the displacement and m_t is the total mass of the box. The column cross-section thickness varied between 1 and 3 mm. The range was mainly dictated by the thicknesses of commercially available Al extrusions. The foam filler relative density ranged between 0 (no filling) and 0.2. The maximum mean constraint load value, 55 kN, was determined by averaging the mean crushing loads of commercially available various Al and steel boxes. The determined maximum mean load constraint is slightly smaller than the one (68.5 kN) used in reference [19].

RSM is a widely used method of structural design optimisation studies and presented as

$$\hat{y} = \text{SEA}(t,\ \rho^*) = \sum_{i=1}^{n} \beta_i \varphi_i(t,\ \rho^*), \tag{5}$$

where φ_i $(t,\ \rho^*)$ is the basic function, n represents the number of basic function and β_i is the regression coefficient. The polynomial form of the basic function is commonly selected, as it yields higher accuracies. A fourth-order (quartic) polynomial function is selected in the optimisation study as

$$\begin{aligned} &1, x_1, x_2, \ldots x_n, x_1^2, x_1x_2, \ldots x_1x_n, \ldots\ldots, x_n^2, x_1^3, x_1^2x_2, \ldots, \\ &x_n^2x_2, \ldots, x_n^3, x_1^4, x_1^3x_2, \ldots, x_1^3x_n, x_1^2x_2^2, \ldots, x_1^2x_n^2, \ldots, \\ &x_1x_2^3, \ldots, x_1x_n^3, \ldots, x_n^4. \end{aligned} \tag{6}$$

The regression coefficient β_i is estimated by the methods of least squares. For m $(m > n)$ observations, the least square function can be written as

$$L = \sum_{i=1}^{m} \varepsilon_i^2 = \sum_{i=1}^{m} \left[y_i - \sum_{j=1}^{n} \beta_j \varphi_j(t, \rho^*) \right]^2, \tag{7}$$

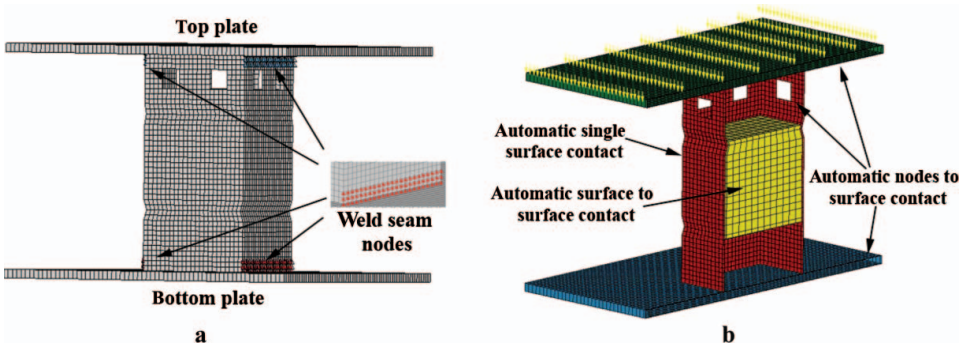

Figure 4. The details of foam-filled crash box model: (a) overall view and (b) cross-sectional view.

where y_i is the response at the selected design points $(t, \rho^*)_i$ from the specified design mesh and ε_i is the error between y_i and RSM approximation of $\hat{y}$ at coincident design point.

Regression coefficient vector, $B = (\beta_i, \beta_2, \beta_n)$, can be determined using, $\frac{\delta L}{\delta \beta} = 0$. Then, B can be calculated as

$$B = (\phi^T \phi)^{-1} \phi^T y, \tag{8}$$

where y is the objective vector, $y = (y_1, y_2, \ldots y_n)$ and ϕ denotes the matrix of basic functions evaluated at m sampling points as

$$\phi = \begin{bmatrix} \varphi_1(t, \rho^*)_1 & \cdots & \varphi_n(t, \rho^*)_1 \\ \vdots & \ddots & \vdots \\ \varphi_1(t, \rho^*)_\mathrm{m} & \cdots & \varphi_n(t, \rho^*)_\mathrm{m} \end{bmatrix}_{\mathrm{mxn}}. \tag{9}$$

By substituting Equation (9) into Equation (5), the response surface model is created and the objective functions SEA (t, p^*) can be determined. Error sum of square (SS_E), total sum of square (SS_T), R^2, adjusted R^2_{adj} and root of mean squared error (RMSE) are calculated. The details of RMS can be found elsewhere [12,13].

An r^s full factorial design was used to generate a mesh of sampling points for the RSM of the partially foam-filled Al crash boxes. The generated sampling mesh consisted of r points spaced at periodic intervals. In order to handle r points of interval, at least $(r+1)^s$ factorial experiments or simulations should be performed. In this study, r and s were selected as 4 and 2, respectively [13].

4. Numerical simulation

The details of the filled box model are shown in Figures 4(a) and 4(b). The 1050H14 Al crash box was modelled using four-node Belytschko-Tsay shell elements with one-point integration in the plane and five in the thickness direction. The foam filler was modelled using eight-node solid elements and the top and bottom montage plates using shell elements. In the model, the translation and rotation of the bottom montage plate was restricted, and the weldments between montage plates and the crash box were simulated by nodal constraints. The width of the welding zone was measured 6 mm; therefore, the rotational motions of the nodes at a distance of 6 mm from the top and bottom of the crash boxes were restricted in all directions (Figure 4(a)). The translation motion of the welding zone nodes was only allowed in the long axis of the box. The self-contacting crash zone surfaces (folds) were modelled using automatic single surface contact algorithm in LS-DYNA (Figure 4(b)). The contacts between foam and box and between foam and montage plates were modelled using automatic surface-to-surface contact (Figure 4(b)). The contact between box and montage plate was modelled with automatic nodes to surface contact algorithm (Figure 4(b)). The static and dynamic friction coefficients were taken as 0.3 and 0.2, respectively.

The box and montage plate materials, 1050H14 and 6061T4 Al, were modelled using plastic-kinematic material model (Mat 3). In plastic-kinematic material model, the mechanical properties are characterised by the material yield strength (σ_o), Young's modulus (E) and tangent modulus (E_t). The yielding is defined by von Mises yield criterion. In plastic-kinematic plasticity algorithm, the flow stress (σ) is given as

$$\sigma = \sigma_o + \beta' E_p \varepsilon^{\mathrm{p}}_{\mathrm{eff}}, \tag{10}$$

where β' is the hardening coefficient and $\varepsilon^{\mathrm{p}}_{\mathrm{eff}}$ and E_p are the effective plastic strain and plastic hardening modulus, respectively. The plastic hardening modulus is calculated using the following relation:

$$E_p = \frac{E E_\mathrm{t}}{E - E_\mathrm{t}}. \tag{11}$$

Al foam fillers, Alulight and Hydro foam, were modelled using honeycomb material model (Mat 26). Honeycomb material model is essentially anisotropic; therefore, the material parameters are required to be determined

Table 1. Tensile mechanical properties of 1050H14 Al alloy.

Young modulus (GPa)	Tangent modulus (MPa)	Yield strength (MPa)	Ultimate tensile strength (MPa)	Failure strain (%)
70	147	105	110	8.4

separately for each direction. Al foams are usually considered nearly isotropic, showing small variations in mechanical properties in three directions; therefore, the mechanical properties in three directions are considered to be the same [15]. The material model further assumes that the foam behaves as a solid and switches to an isotropic elastic-perfectly plastic material with von Mises yield criterion after densification strain. Thus, densification strain of foam material should be described for Al foam modelling using Mat 26. Mat 26 foam model properties of Alulight and Hydro Al foam were determined using the compression stress–strain curves predicted by Deshpande and Fleck foam model.

The quasi-static crushing simulations in LS-DYNA require mass scaling. Two methodologies of mass scaling are generally applied [16]: scaling down the material density (the total time of solution is decreased by increasing the loading rate of quasi-static simulation) and scaling up the mass density at very low loading rates (very large time steps). In quasi-static simulation using mass scaling, two conditions must be satisfied. The total kinetic energy must be very small compared with total internal energy and the load-displacement curves must be independent of deformation rate. The above conditions were found to be satisfied in the quasi-static simulations of the empty and filled boxes by scaling down the material mass density by a factor of 1000 at 2 m s^{-1} deformation rate.

5. Results and discussion

Tensile mechanical properties of 1050H14 Al parallel to the extrusion direction are tabulated in Table 1. The alloy shows a ductility of 8.4% and a proof strength of 105 MPa parallel to the extrusion direction. The plastic-kinematic hardening material model parameters of 6061T4 Al alloy were taken from reference [9] and are tabulated in Table 2. The compression stress–strain curves of Alulight foams at various relative densities are shown in Figure 5(a). Each curve in this figure represents average stress values of three repetitive tests. The plateau stress is determined by simply averaging the stress values between the initial collapse strain and 0.1 strain. The determined experimental plateau stress values are then fitted with a power law strengthening equation as (Figure 5(b))

Table 2. Plastic-kinematic hardening material model (MAT 3) parameters of 6061T4 Al [9].

Young modulus (GPa)	Tangent modulus (MPa)	Yield strength (MPa)
70	450	110.3

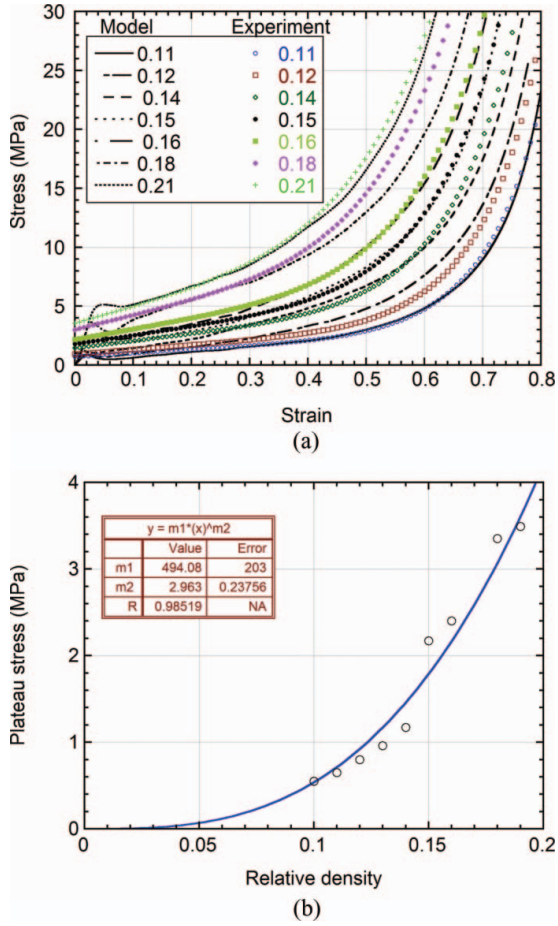

Figure 5. (a) Experimental and calculated compression stress–strain curves and (b) plateau stress–relative density curve of Alulight foam.

$$\sigma_P = C_1(\rho^*)^{n'}. \tag{12}$$

The values of C_1 and n' are found to be 494.08 and 2.963 MPa, respectively. The foams with 0.11 (297 kg m^{-3}) and 0.15 (405 kg m^{-3}) relative density were used to fill Al crash boxes for compression testing. The plateau stresses of the foam at 0.11 and 0.15 relative densities are determined to be 0.65 and 2.17 MPa, respectively. The determined Deshpande and Fleck foam model parameters of Alulight foam are further tabulated in Table 3 and the foam model stress–strain curves are shown in Figure 5(a) together with experimental stress–strain curves. Deshpande and Fleck foam model parameters of Hydro foam (AlSi8Mg) taken from reference [14] are tabulated in Table 4.

The experimental and simulation load and mean load-displacement curves of empty and filled crash boxes are

Table 3. Deshpande and Fleck foam model constants of Alulight foam.

Model description: $\{\sigma_p, \alpha_2, \gamma, \frac{1}{\beta}\} = C_0 + C_1(\frac{\rho_f}{\rho_{fo}})^{n'}$				
Parameter	σ_p (MPa)	α_2 (MPa)	$1/\beta$	γ (MPa)
C_0	0	0	0.14307	0
C_1	494.08	125.44	97.396	298.2
n'	2.963	0.6635	4.0628	2.0563

Table 4. Deshpande and Fleck foam model constants of Hydro Al foam [14].

Model description: $\{\sigma_p, \alpha_2, \gamma, \frac{1}{\beta}\} = C_0 + C_1(\frac{\rho_f}{\rho_{fo}})^{n'}$				
Parameter	σ_p (MPa)	α_2 (MPa)	$1/\beta$	γ (MPa)
C_0	0	0	0.22	0
C_1	590	140	320	40
n'	2.21	0.45	4.66	1.4

shown in Figure 6 as a function of box wall thickness and foam filler density. Deformation load levels of the simulations generally show close agreements with those of experiments in 2- and 3-mm-thick boxes, while the simulation mean load values are slightly higher than experimental values in 2.5-mm-thick boxes. The experimental and simulation deformation pictures of 3-mm-thick empty and filled boxes are shown sequentially in Figures 7(a) and 7(b). The folding in all boxes begins, both experimentally and numerically, from the corrugated section (A in Figure 7(a)). The weldments of the boxes are noted mostly intact during compression. In a few crushed boxes, cracks extending several millimetres in the weld section are seen (Figure 7(a)); however, no significant effect of cracks is found on the load-displacement curves of the boxes. In empty boxes, in total two folds form both experimentally and numerically, while foam filling increases the number of folds to three. Foam filling induces a shorter fold length by restraining inward folding of the box wall.

Simulation load-displacement and mean load-displacement curves of empty and partially foam-filled 3-mm-thick 1050H14 Al crash boxes are shown in Figure 8(a). In the initial deformation region of the curves, the foam filling increases both load and mean load values moderately until about 60 mm displacement (50% deformation). The deformation load values sharply increase above 60 mm displacement as the foam filler is compressed uniaxially between the compression platens. It is also noted that the increase in the load values of the 0.2 relative density foam-filled box starts earlier than the 0.1 relative density foam-filled box. The effect of Hydro foam filling on the crushing and mean load of 1050H14 box is

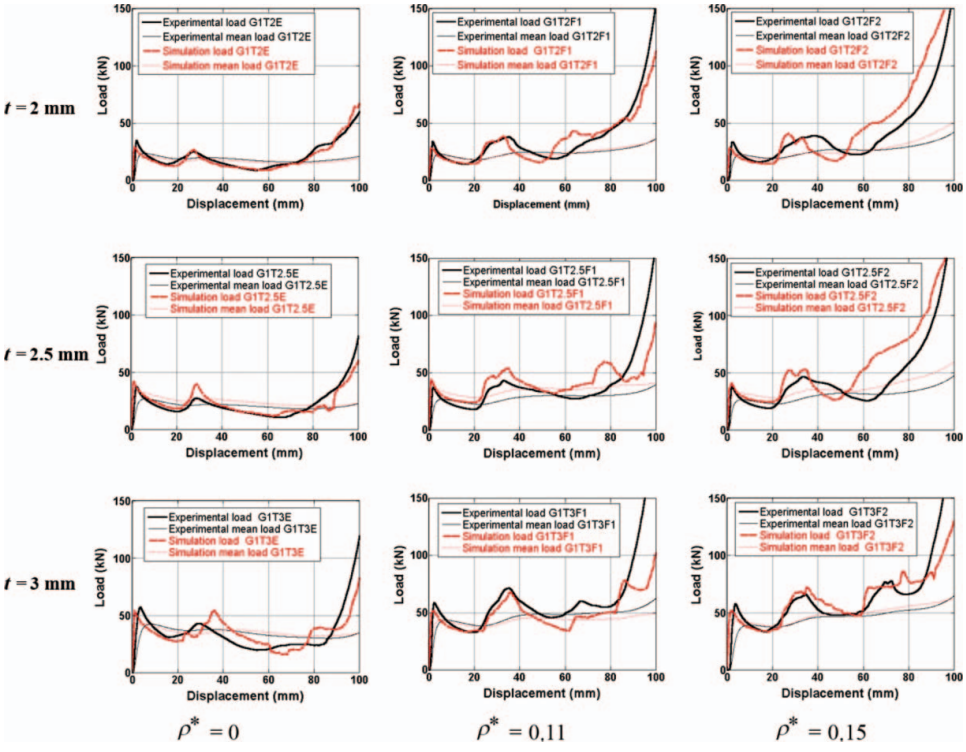

Figure 6. Experimental and simulation load and mean load-displacement curves of crash boxes as function of box wall thickness and foam filler relative density.

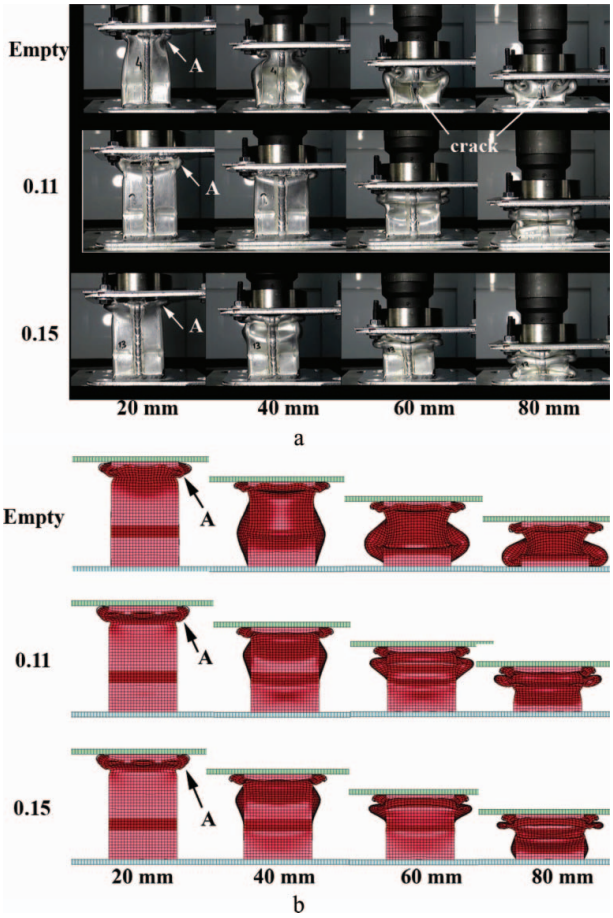

Figure 7. (a) Experimental and (b) simulation deformation pictures of 3-mm-thick empty and filled boxes.

shown in Figure 8(b). As with Alulight foam filling, the load values of Hydro foam-filled 1050H14 Al crash box increase sharply after about 60 mm displacement. Hydro foam filling induces a higher crushing load than Alulight foam filling as noted in Figure 8(b). Representative load-displacement curve of partially Alulight foam-filled 3-mm-thick 6061T4 Al box is shown in Figure 8(c). Similar to 1050H14 Al boxes, Alulight foam filling of 6061T4 Al box results in higher load values than those of empty box, as is expected. However, the increase in load values of filled tubes after about 60 mm displacement is more pronounced in 6061T4 Al boxes (Figure 8(c)). The simulated cross-section deformation patterns of 1050H14 Al empty, 0.1 relative density foam-filled and 0.2 relative density foam-filled crash boxes at increasing displacements are shown in Figures 9(a)–9(c), respectively. As is noted in Figures 9(b) and 9(c), the foam filler axial l compression starts before 60 mm displacement. The main reason for that is the foam filler axial and also lateral deformation between the folds, which reduces the length of the foam filler (Figure 10). This also proves an interaction between foam filler and box wall. The simulated deformation

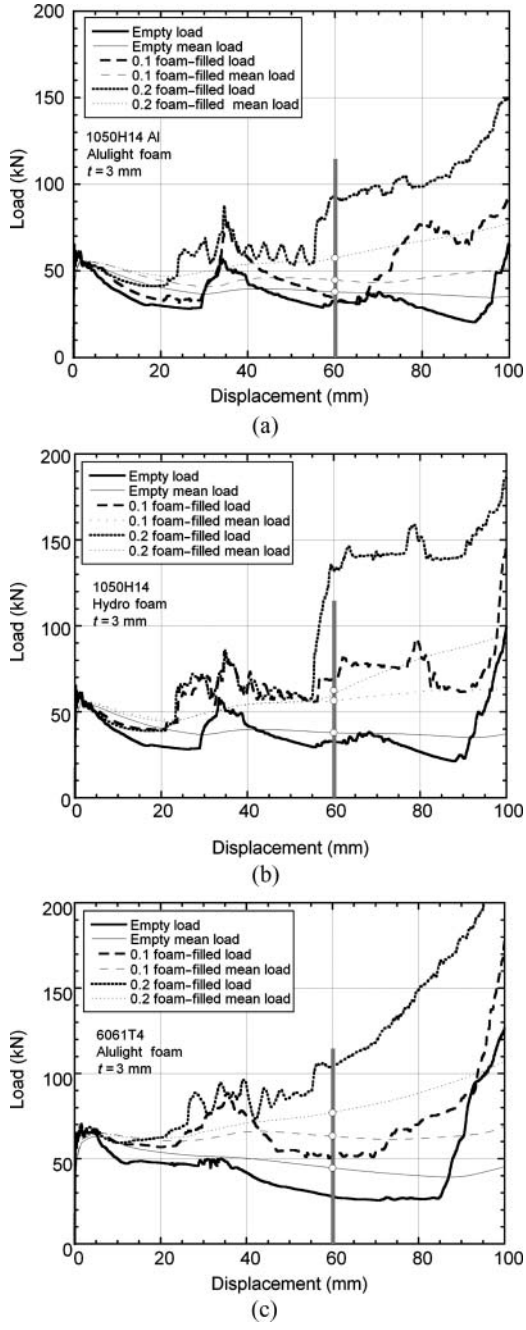

Figure 8. Simulation load-displacement and mean load-displacement curves of 3-mm-thick (a) Alulight foam-filled 1050H14 Al crash box, (b) Hydro foam-filled 1050H14 Al crash box and (c) Alulight foam-filled 6061T4 Al crash box.

pattern and critical deformation for the foam filler axial compression were found to be the same for Hydro and Alulight foam-filled crash boxes.

The variations of mean load and SEA values of Alulight foam-filled 1050H14 Al crash box with foam relative density at 50% deformation are shown in Figures 11(a) and 11(b), respectively. The mean load values tend to increase

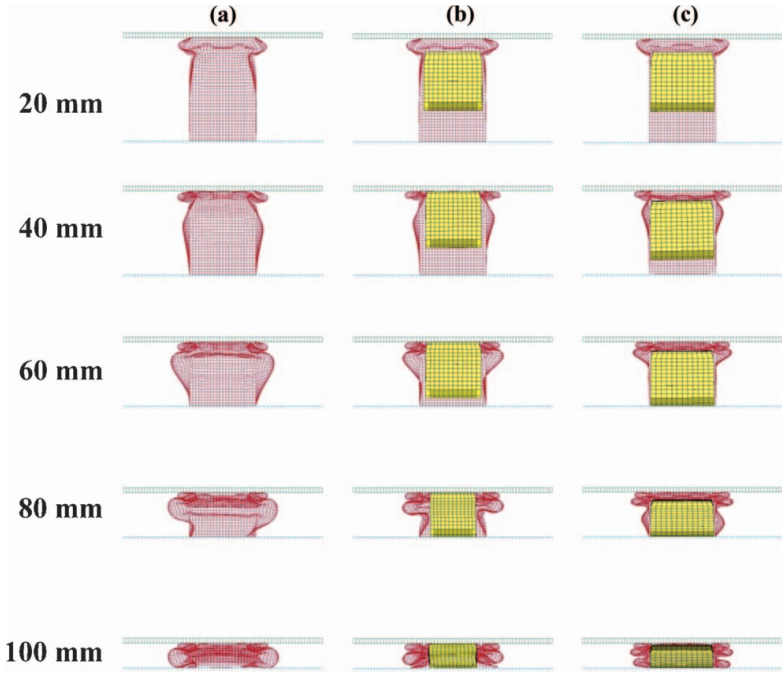

Figure 9. Simulation deformed shapes of (a) empty, (b) 0.1 and (c) 0.2 relative density foam-filled 1050H14 Al crash box at various displacements.

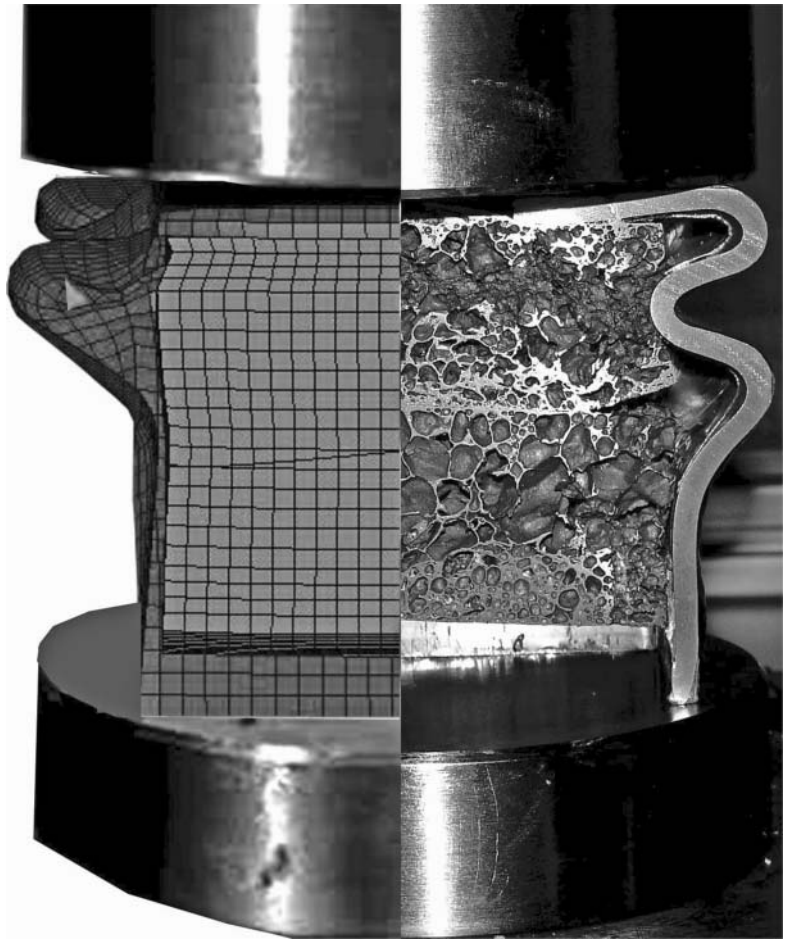

Figure 10. 3 mm thick 0.15 foam-filled crash box showing axial deformation of the foam filler between the folds (50 mm displacement).

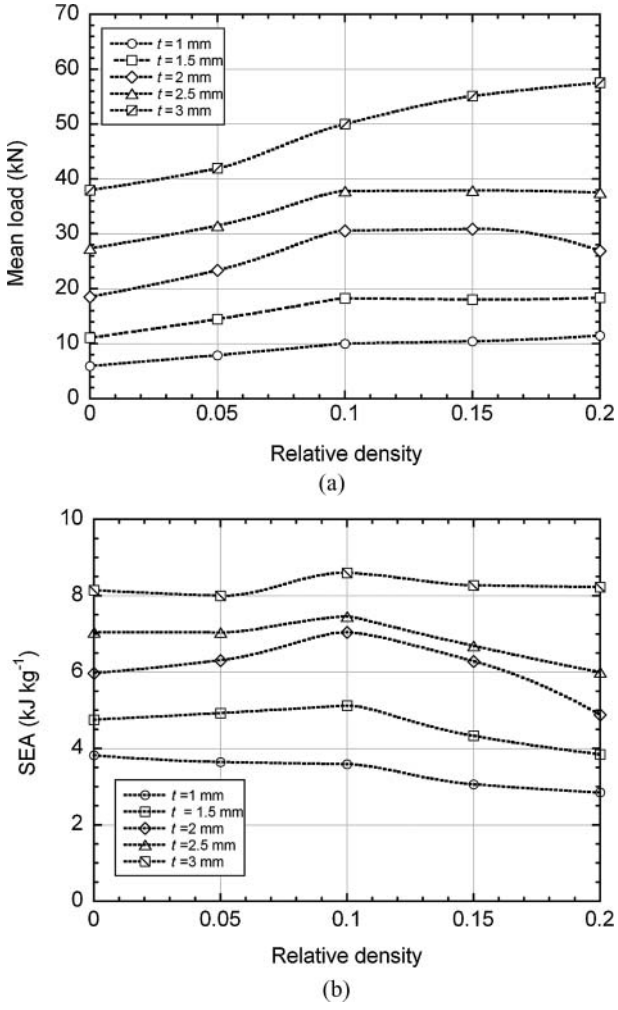

Figure 11. The variation of (a) mean load and (b) SEA values of 1050H14 Al crash boxes with foam relative density and box wall thickness.

with increasing foam relative density (Figure 11(a)). SEA values, however, show maxima at 0.1 foam relative density as seen in Figure 11(b). Similar trends of mean load and SEA values of Hydro foam-filled 1050H14 Al crash box and Hydro and Alulight foam-filled 6061T4 Al crash boxes with foam relative density were also found.

The constructed response surface of mean load–box wall thickness–foam relative density graphs of Alulight and Hydro foam-filled 1050H14 and 6061T4 Al boxes are shown sequentially in Figures 12(a) and 12(b). For both Alulight and Hydro foam filling, 6061T4 Al crash boxes result in higher mean load values, emphasising the effect of crash box material strength on the mean load values. The response surface of SEA–box wall thickness–foam relative density graphs of Alulight and Hydro foam-filled 1050H14 Al and 6061T4 Al boxes are further shown sequentially in Figures 13(a) and 13(b). The SEA values of filled 6061T4 Al crash box are again higher than those of 1050H14 Al

Table 5. R^2, R^2_{adj} and RMSE values for RMS of partially foam-filled crash box.

Crash box	Response function	R^2	R^2_{adj}	RMSE
1050H14 + Alulight foam	Mean load	0.9958	0.9954	0.9912
	SEA	0.9966	0.9963	0.1098
6061T4 + Alulight foam	Mean load	0.9988	0.9987	0.7193
	SEA	0.9967	0.9964	0.1400
1050H14 + Hydro foam	Mean load	0.9964	0.9961	1.0290
	SEA	0.9896	0.9887	0.2289
6061T4 + Hydro foam	Mean load	0.9992	0.9992	0.6379
	SEA	0.9965	0.9962	0.1630

crash box. It is also noted that Hydro foam filling is more effective than Alulight foam filling in increasing both mean load and SEA values of filled boxes, resulting from relatively higher plateau stresses of Hydro foam. Values of R^2, R^2_{adj} and RMS for filled crash boxes response functions are tabulated in Table 5. High values of R^2 and R^2_{adj} tabulated in Table 5 show that the fitted quadratic objective functions effectively represent the mean load and SEA values of the crash boxes investigated. The RMSE values of Alulight and Hydro foam-filled 1050H14 Al crash boxes are also higher than those of Alulight and Hydro foam-filled 6061T4 Al crash boxes.

The optimum box thickness and foam relative density of filled boxes with the tube wall thickness and mean crushing load constraints are tabulated in Table 6. It is noted in Table 6 that higher yield strength of box material and higher plateau stresses of filler result in higher SEA values at smaller box wall thickness and foam relative density. The highest SEA value (11.37 kJ kg^{-1}) is found in Hydro foam-filled 6061T4 Al crash box with an optimum wall thickness of 2.77 mm and a foam filler relative density of 0.047. The optimum SEA of Alulight foam-filled 6061T4 Al crash box is 10.14 kJ kg^{-1} at a wall thickness of 2.84 mm and a foam filler relative density of 0.088. The optimum SEA value of 1050H14 Al crash box is reached at a tube thickness of 3 mm (upper constraint of tube thickness) with a foam relative density of 0.051 and 0.11 for Hydro and Alulight foam filling, respectively. The variations of mean load and SEA values of 1050H14 and 6061T4 Al empty crash boxes with wall thickness are shown in Figure 14. It is noted that at the

Table 6. Optimum thickness and relative foam density of partially Alulight and Hydro foam-filled 1050H14 and 6061T4 Al boxes.

	1050H14 + Alulight	6061T4 + Alulight	1050H14 + Hydro	6061T4 + Hydro
t (mm)	3	2.8389	3	2.7659
ρ^*	0.1114	0.0878	0.0508	0.0471
SEA (kJ kg^{-1})	8.5648	10.1439	9.8894	11.3723

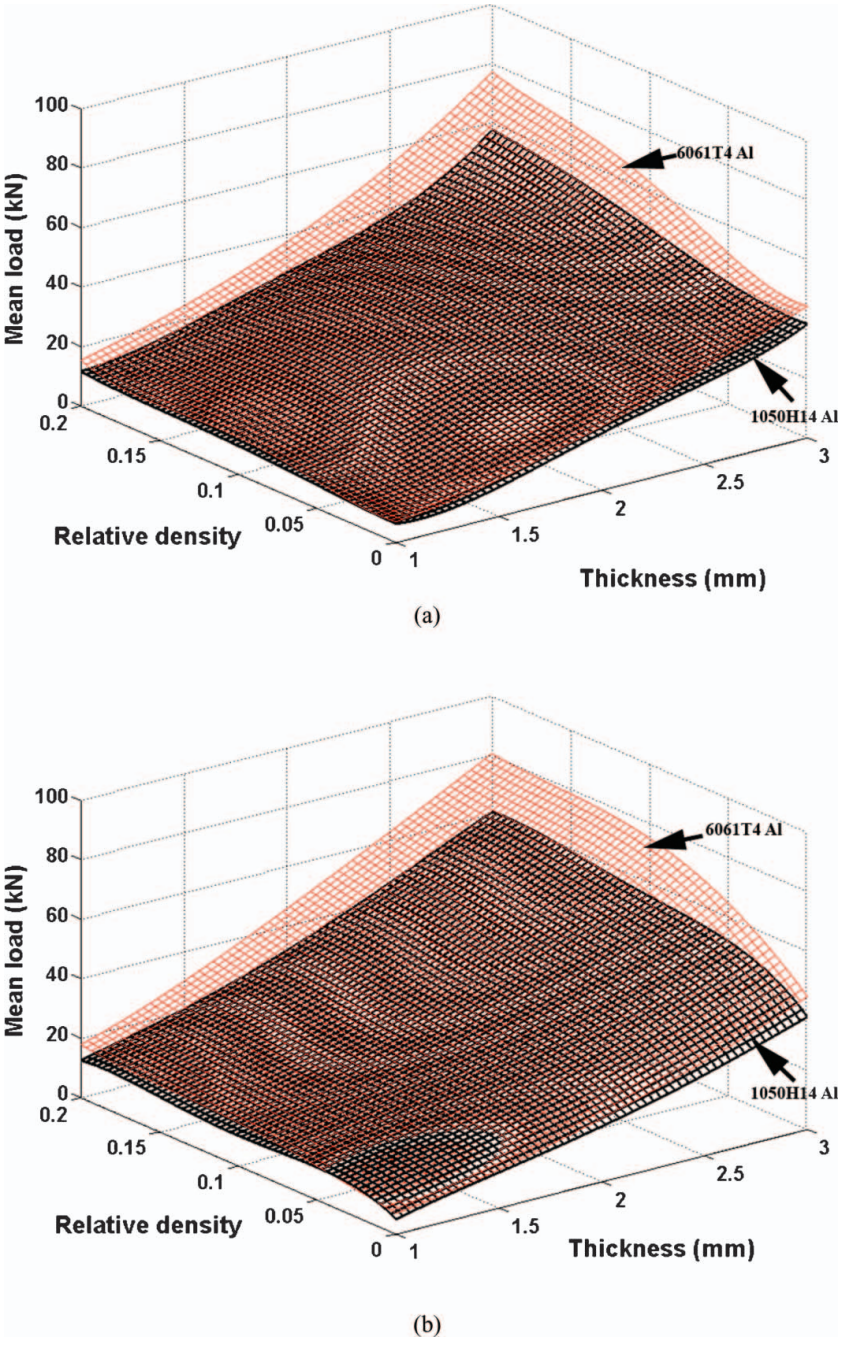

Figure 12. Response surface of mean load of filled boxes: (a) Alulight and (b) Hydro foam filling.

maximum constraint mean load value (55 kN), the thickness of the empty boxes is greater than 3 mm, 3.45 mm for 6061T4 and 3.88 mm for 1050H14 Al crash box. The SEA values of 6061T4 and 1050H14 Al crash box at 3 mm wall thickness are 9.50 and 8.11 kJ kg^{-1}, respectively. In order to compare the energy absorption of empty tube with partially foam-filled tubes, the variations of the energy absorption of empty crash boxes (50% deformation) with weight are shown in Figures 15(a) and 15(b) for 1050H14 and 6061T4 crash box, respectively. On the same graph, the variations of empty tube thicknesses with weight and the energy absorption values (50% deformation) of optimised foam-filled boxes as function of total weight of the filled crash boxes are also shown. When the crash box of 3 mm thickness constraint is considered, 1050H14 and 6061T4 Al empty boxes absorb total energies of 2.21 and 2.58 kJ, respectively (Figures 15(a) and 15(b)). Alulight and Hydro Al foam-filled optimised 1050H14 crash boxes absorb total energies of

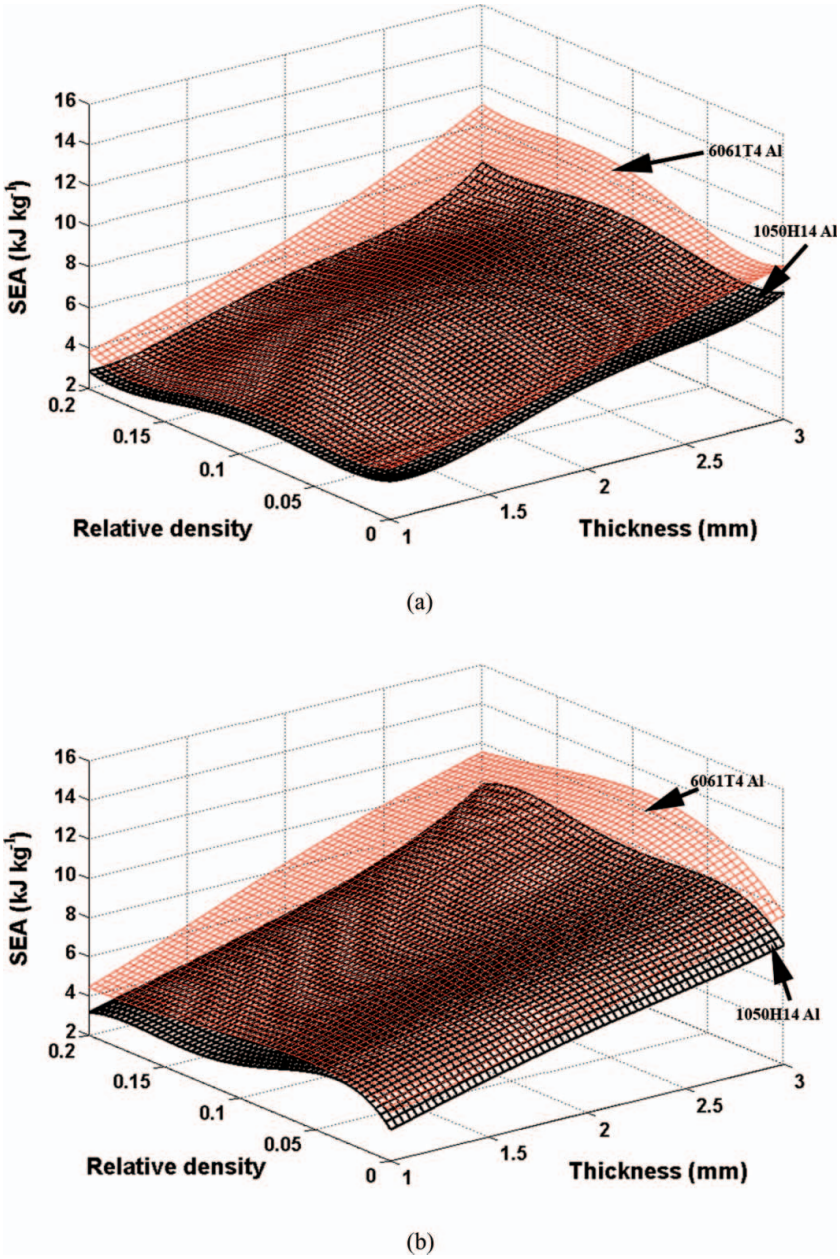

Figure 13. Response surface of SEA of filled boxes: (a) Alulight and (b) Hydro foam filling.

3.12 and 3.06 kJ at the same thickness (Figure 15(a)), with 33% and 12.7% increase in the total weight and about 40% increase in total energy absorption as compared with empty 1050H14 crash box, respectively. The optimised Alulight and Hydro foam-filled 6061T4 crash boxes increase the energy absorption to 3.26 and 3.41 kJ, with 22% and 4.3% increase in the total weight and 26% and 30% increase in the total energy absorption as compared with empty 6061T4 crash boxes, respectively. When the thickness constraint is exceeded, empty 1050H14 and 6061T4 Al boxes are about 35% and 21% energetically more efficient than Alulight foam-filled 1050H14 and 6061T4 Al boxes at the optimum foam-filled and equal weight condition, respectively. While Hydro foam filling of 1050H14 and 6061T4 crash boxes results in 13% and 23.5% increase in energy absorption at equal weight basis as compared with empty counterparts, respectively.

Above results clearly show that partial foam filling of commercial crash boxes can also increase both SEA and mean load values, at relatively low displacements. This effect results from the foam filler axial and also lateral deformation in between the progressing folds of the crash

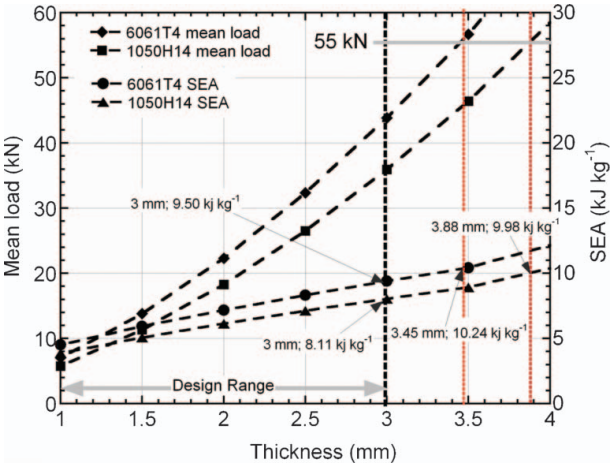

Figure 14. Mean load and SEA change versus thickness of empty 1050H14 and 6061T4 Al crash box.

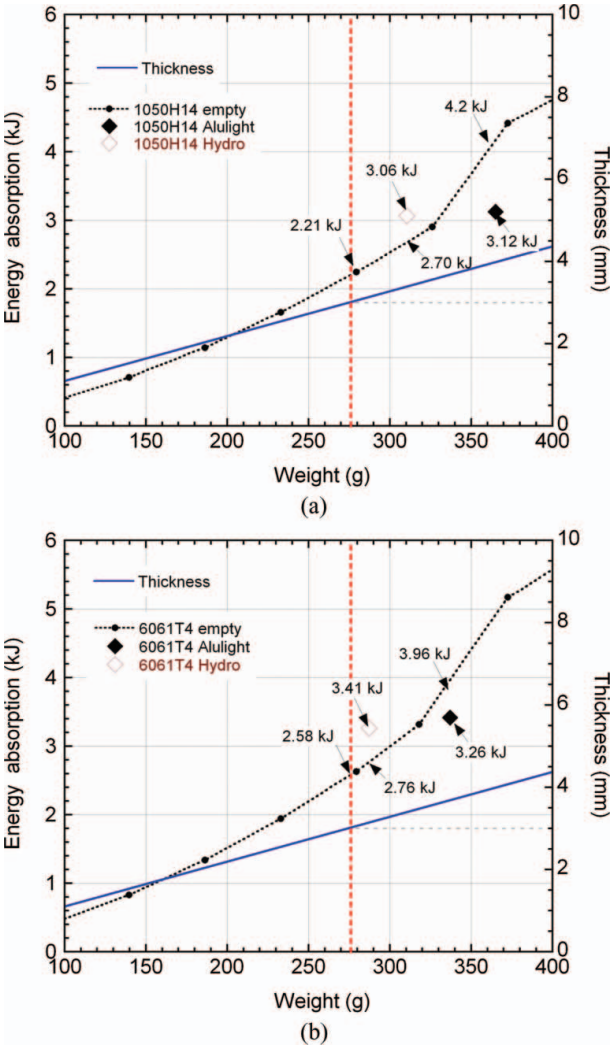

Figure 15. The variation of empty tube energy absorption (at 50% deformation) and thickness with weight, and the optimum energy absorption versus weight data of filled tubes: (a) 1050H14 and (b) 6061T4.

box which is observed both numerically and experimentally (Figures 9 and 10). The effect is further elevated when a higher yield strength box wall material and foam filler and foam filler relative density is used. The optimisation schedule would also be necessary to maximise SEA values of the partial foam-filled crash box against box wall thickness, foam filler density and maximum allowable mean load values.

6. Conclusions

Partially Alulight and Hydro closed-cell foam-filled commercial 1050H14 Al and 6061T4 Al crash boxes were optimised in order to maximise SEA values with the following constraints: a maximum mean load of 55 kN, box thickness between 1 and 3 mm and the foam filler relative densities between 0 (no filling) and 0.2. The constraint maximum mean load value was determined by averaging the mean crushing loads of commercially available various Al and steel boxes. The simulated quasi-static crushing of empty and filled crash boxes using LS-DYNA was further confirmed with experimental quasi-static crushing testing of empty and Alulight foam-filled commercial 1050H14 Al crash boxes. Results showed that partial foam filling of commercial crash boxes increased both SEA and mean load values because of foam filler axial and lateral deformation in between the progressing box wall folds. Within the studied constraint range of box mean load, box wall thickness and foam filler density, Alulight and Hydro foam-filled optimised 1050H14 and 6061T4 crash boxes resulted in 26%–40% increase in total energy absorption as compared with empty crash boxes. At the same weight basis, the use of a higher yield strength box wall material and foam resulted in higher energy absorption in partial foam-filled boxes at relatively low displacements.

Acknowledgement

The authors would like to thank the Scientific and Technical Council of Turkey (TUBITAK) for the grant no. 106M186.

References

[1] ASTM Standard E8/E8M-08, *Standard Test Methods for Tension Testing of Metallic Materials*, ASTM International, West Conshohocken, PA, 2003.

[2] M. Avalle, G. Chiandussi, and G. Belingardi, *Design optimization by response surface methodology: Application to crashworthiness design of vehicle structures*, Struct. Multidiscip. Optim. 24 (2002), pp. 325–332.

[3] T. Borvik, O.S. Hopperstad, A. Reyes, M. Langseth, G. Solomos, and T. Dyngeland, *Empty and foam-filled circular aluminium tubes subjected to axial and oblique quasistatic loading*, Int. J. Crashworthiness 8 (2003), pp. 481–494.

[4] G. Chiandussi and M. Avalle, *Maximisation of the crushing performance of a tubular device by shape optimisation*, Comput. Struct. 80 (2002), pp. 2425–2432.

[5] Y.-B. Cho, C.-H. Bae, M.-W. Suh, and H.-C. Sin, *A vehicle front frame crash design optimization using hole-type and dent-type crush initiator*, Thin Wall Struct. 44 (2006), pp. 415–428.
[6] V.S. Deshpande and N.A. Fleck, *Isotropic constitutive models for metallic foams*, J. Mech. Phys. Solids 48 (2000), pp. 1253–1283.
[7] M. Giess and J. Tomas, *Improving safety performance in frontal collisions by changing the shape of structural components*, 16th ESV Conference, Windsor, Canada, Paper Number 98-S1-O-07, National Highway Traffic Safety Administration, Washington D.C., 1998, pp. 222–228.
[8] A.G. Hanssen, O.S. Hopperstad, M. Langseth, and H. Ilstad, *Validation of constitutive models applicable to aluminium foams*, Int. J. Mech. Sci. 44 (2002), pp. 359–406.
[9] S. Hou, Q. Li, S. Long, X. Yang, and W. Li, *Multiobjective optimization of multi-cell sections for the crashworthiness design*, Int. J. Impact Eng. 35 (2008), pp. 1355–1367.
[10] H.S. Kim, W. Chen, and T. Wierzbicki, *Weight and crash optimization of foam-filled three-dimensional 'S' frame*, Comput. Mech. 28 (2002), pp. 417–424.
[11] Y. Liu, *Crashworthiness design of multi-corner thin-walled columns*, Thin Wall Struct. 46 (2008), pp. 1329–1337.
[12] D.C. Montgomery, *Design of Experiments*, John Wiley & Sons, New York, 2001.
[13] H.R. Myers and D.C. Montgomery, *Response Surface Methodology: Process and Product Optimization Using Designed Experiments*, John Wiley & Sons, New York, 1995.
[14] A. Reyes, O.S. Hopperstad, T. Berstad, A.G. Hanssen, and M. Langseth, *Constitutive modeling of aluminum foam including fracture and statistical variation of density*, Eur. J. Mech. A/Solid 22 (2003), pp. 815–835.
[15] S. Santosa and T. Wierzbicki, *Crash behavior of box columns filled with aluminum honeycomb or foam*, Comput. Struct. 68 (1998), pp. 343–367.
[16] S.P. Santosa, T. Wierzbicki, A.G. Hanssen, and M. Langseth, *Experimental and numerical studies of foam-filled sections*, Int. J. Impact Eng. 24 (2000), pp. 509–534.
[17] H.R. Zarei and M. Kröger, *Bending behavior of empty and foam-filled beams: Structural optimization*, Int. J. Impact Eng. 35 (2008), pp. 521–529.
[18] H.R. Zarei and M. Kröger, *Multiobjective crashworthiness optimization of circular aluminum tubes*, Thin Wall Struct. 44 (2006), pp. 301–308.
[19] H.R. Zarei and M. Kröger, *Optimization of the foam-filled aluminum tubes for crush box application*, Thin Wall Struct. 46 (2008), pp. 214–221.
[20] H. Zarei and M. Kröger, *Optimum honeycomb filled crash absorber design*, Mater. Des. 29 (2008), pp. 193–204.
[21] X. Zhang, G. Cheng, B. Wang, and H. Zhang, *Optimum design for energy absorption of bitubal hexagonal columns with honeycomb core*, Int. J. Crashworthiness 13 (2008), pp. 99–107.